THE AMERICAN SOCIETY OF MECHANICAL ENGINEERS
345 E. 47th St., New York, N.Y. 10017

98-GT-485

PREDICTION OF RESONANT RESPONSE OF SHROUDED BLADES WITH 3D SHROUD CONSTRAINT

B. D. Yang, J. J. Chen and C. H. Menq*

Department of Mechanical Engineering
The Ohio State University
Columbus, OH 43210
U.S.A.

* Corresponding Author (614)292-4232

ABSTRACT

In this paper, the 3D shroud contact kinematics of a shrouded blade system is studied. The assumed blade motion has three components, namely axial, tangential, and radial components, which result in a three dimensional relative motion across the shroud interface. The resulting relative motion can be decomposed into two components. The first one is on the contact plane and can induce stick-slip friction. The other component is perpendicular to the contact plane and can cause variation of the contact normal load and, in extreme circumstances, separation of the two contacting surfaces. In order to estimate the equivalent stiffness and damping of the shroud contact an approach is proposed. In this approach, the in-plane slip motion is assumed to be elliptical and is decomposed into two linear motions along the principal major and minor axes of the ellipse. A variable normal load friction force model (Yang and Menq, 1996) is then applied separately to each individual linear motion, and the equivalent stiffness and damping of the shroud contact can be approximately estimated. With the estimated stiffness and damping, the developed shroud contact model is applied to the prediction of the resonant response of a shrouded blade system. The effects of two different shroud constraint conditions, namely 2D constraint and 3D constraint, on the resonant response of a shrouded blade system are compared and the results are discussed.

INTRODUCTION

In the turbine jet engine industry, shrouds are often employed in turbine design to attenuate blade vibration and at the same time to increase aeroelatistic stability of the turbine. During the engine operation, the shrouded fan blades rotate through the fluid flow with severe fluctuation, and as a result, the blades vibrate and experience friction constraint at the shroud contact. During a cycle of motion, the shroud contact point experiences alternating stick-slip friction force that adds friction damping as well as additional spring force to the system (Cameron *et al*, 1990; Ferri, 1996; Griffin, 1980). Therefore, in order to analytically evaluate the performance of the shroud and to help the design, there is a need to consider this 3D shroud constraint so that the resulting resonant frequencies and vibration magnitudes of the shrouded blades can be accurately estimated.

The protruding shrouds constrain the blade motions not only along the contact plane but also along the normal direction of the plane, resulting in complex contact kinematics, in which the relative motion has two components: in-plane tangential motion on the contact plane and normal component perpendicular to the contact. The in-plane tangential relative motion is two-dimensional, and it can induce stick-slip friction (Yang and Menq, 1996). On the other hand, the normal relative motion can cause variation of the contact normal load and, in extreme circumstances, separation of the two contacting surfaces, an effect which cannot be adequately modeled by a simple friction contact model having constant normal load (Griffin, 1980). In our prior study (Yang and Menq, 1996), a 2D version of shroud contact kinematics was investigated, in which the interface retains the normal component of the relative motion that causes normal load variation, while the in-plane tangential component of the relative motion degenerates into linear motion. This simplification is the result of neglecting the radial component of the blade motion and can be regarded as the first step towards understanding the effect of shroud contact kinematics on the resonant response of a shrouded blade system. In other words, in this shroud contact model, the assumed blade motion has only two components, namely axial and tangential components. These two components results in a relative motion which has linear trajectory on the shroud contact plane and has the other component perpendicular to the shroud contact plane. Since shrouds protrude from the sides of the airfoils, the radial component of the relative motion of the shroud contact may become as important as the other two components. If this is the case, the actual relative motion on the shroud contact plane will have an elliptic trajectory rather than a

Presented at the International Gas Turbine & Aeroengine Congress & Exhibition
Stockholm, Sweden — June 2–June 5, 1998
This paper has been accepted for publication in the Transactions of the ASME
Discussion of it will be accepted at ASME Headquarters until September 30, 1998

linear one. Since the effective stiffness of the friction interface and the energy dissipated by friction are strongly effected by the relative motion between the two contact surfaces, the assumed trajectory of the relative motion becomes very important to the prediction of the resonant amplitude and frequency of the shrouded blade system. In other worlds, assuming a linear trajectory imposes a rather severe limitation on the predictive ability of the current approach.

In this paper, the 3D shroud contact, including contact geometry and kinematics, of a shrouded blade system is studied. The assumed blade motion has three components, namely axial, tangential, and radial components. At the shroud contact, these three components results in a three dimensional relative motion which has a two dimensional trajectory on the shroud contact plane and the other component perpendicular to the contact plane. It is apparent that the two components of the in-plane two dimensional slop motion are coupled together when inducing stick-slip friction. However, the coupling effect of a two dimensional relative motion having variable normal load on the stick-slip phenomenon is not well understood at this stage. To estimate the equivalent stiffness and damping of the shroud contact experiencing a two dimensional slip motion and a variable normal load, the first attempt of this study is to use an approximate approach. In this approach, the in-plane slip motion is assumed to be elliptical and is decomposed into two linear motions along the principal major and minor axes of the ellipse. A variable normal load friction force model (Yang and Menq, 1996) is then applied separately to each individual linear motion, and the equivalent stiffness and damping of the shroud contact can be approximately estimated. With the estimated stiffness and damping, the developed shroud contact model can be applied to the prediction of the resonant response of a shrouded blade system. In this paper, the effects of two different shroud constraint conditions, namely 2D constraint and 3D constraint, on the resonant response of a shrouded blade system are compared and the results are discussed.

3D SHROUD CONTACT

In the analysis of a shrouded bladed system, a great simplification can be obtained by assuming that the bladed system is tuned, namely each blade of the system has exactly the same dynamic characteristics. In addition, the excitation of interest is that induced by the blades rotating through circumferential variations in the flow field. It can be shown that in effect each blade is exposed to a periodic excitation having the same amplitude but differing in phase by an amount which is proportional to the blade's angular location on the disk. It is assumed that the resonant response of the bladed system is also periodic and has the same fundamental period as the excitation. Thus the external excitation and the motions of the blades as well as the nonlinear constrained forces can be represented by infinite Fourier series. By truncating these series after the fundamental terms, an approximate solution assuming that the resonant response is simply harmonic can be derived (Menq and Griffin, 1985, Menq *et al*, 1986, Yang and Menq, 1996). In this approach, each blade vibrates in the same manner but with an interblade phase difference (φ) from its adjacent blades. The interblade phase angle is defined as follows:

$$\varphi = \frac{2\pi E}{N} \qquad (1)$$

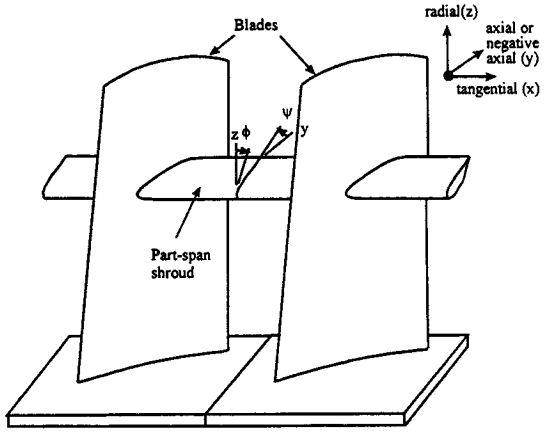

Figure 1 Contact geometry of a shrouded blade system.

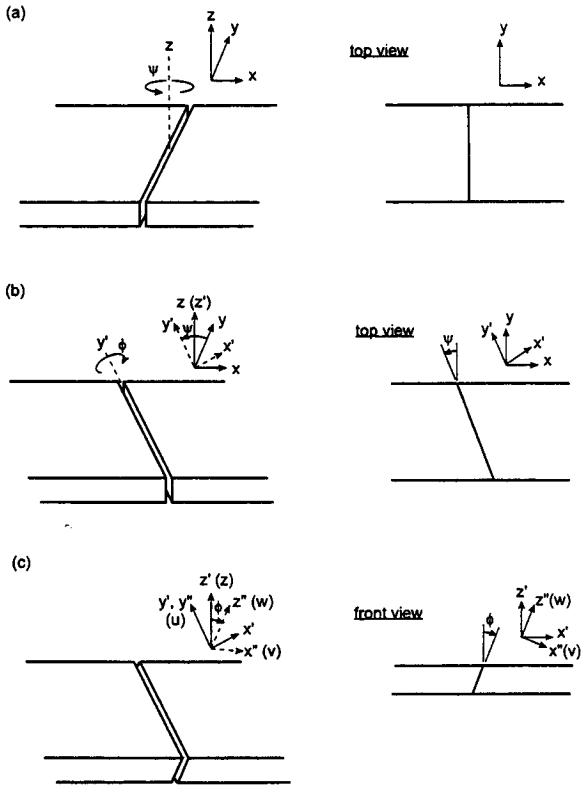

Figure 2 Definition of shroud angle ψ and inclined angle ϕ.

where N is the total number of the blades in the system and E is the engine order of the excitation on the system.

Contact Geometry

Figure 1 shows two shrouded blades contact each other through their protruding shrouds and the *xyz* coordinate system is defined in accordance with the tangential (x), axial (y or $-y$), and radial (z) directions. The geometry of the 3D shroud contact is defined by

two angles ψ (called shroud angle) and ϕ (called inclination angle), whose detailed definitions are shown in Fig. 2. First, a shroud contact plane with its normal pointing towards the x axis is shown in Fig. 2(a). By orienting the contact plane a ψ angle with respect to the z axis, a new contact plane is obtained and shown in Fig. 2(b). The $x'y'z'$ coordinate system associates with this oriented plane, and its x' axis is along the normal direction of the plane and the y' and z' axes are on the plane. The final geometry of the 3D shroud contact can be obtained by rotating the oriented plane again a ϕ angle with respect to the y' axis, and the configuration is shown in Fig. 2(c). The $x''y''z''$ (or uvw) coordinate system associates with this oriented plane, and its x'' (v) axis is along the normal direction of the plane and the y'' (u) and z'' (w) axes are on the plane. In this paper, the global coordinate system is specified by three basis unit vector, namely $[\hat{\mathbf{x}}\ \ \hat{\mathbf{y}}\ \ \hat{\mathbf{z}}]$, and the local coordinate system is defined as $[\hat{\mathbf{v}}\ \ \hat{\mathbf{u}}\ \ \hat{\mathbf{w}}]$. These two coordinate systems can be related to each other as follows.

$$[\hat{\mathbf{v}}\ \ \hat{\mathbf{u}}\ \ \hat{\mathbf{w}}] = [\hat{\mathbf{x}}\ \ \hat{\mathbf{y}}\ \ \hat{\mathbf{z}}]\mathbf{T}_0 \tag{2}$$

where $\mathbf{T}_0$ is the coordinate transformation matrix.

$$\mathbf{T}_0 = \begin{bmatrix} \cos\psi\cos\phi & -\sin\psi & \cos\psi\sin\phi \\ \sin\psi\cos\phi & \cos\psi & \sin\psi\cos\phi \\ -\sin\phi & 0 & \cos\phi \end{bmatrix} \tag{3}$$

In current design practice, the inclination angle ϕ is often set to be zero.

Contact Kinematics

Figure 3 depicts two neighboring blades of a shrouded blade system, whose protruding shrouds are brought into contact with their neighboring shrouds by the centrifugal force during the engine operation. A "substructure" can be used to represent the friction interface that contains the contact plane and small portions of the two neighboring shrouds. Compared to the otherwise massive structure, the substructure can be modeled as two massless elastic elements that are held together by a preload n_0. The points A and B, which are located almost at the ends of the protruding shrouds, are the outermost points of these two elastic elements; and the difference of their respective motions can describe the relative motion of the two neighboring shrouds. When the beam-like turbine blade is subjected to excitation during the engine operation, the twisting action of the blade can cause the points A and B to vibrate in the tangential and axial directions, while the bending action can cause the points A and B to vibrate in the radial direction. Therefore, the motion of the two points are three dimensional.

In this paper, the three dimensional motion is limited to the one having an elliptical trajectory in the 3D space and can be represented as a coordinate vector as follows.

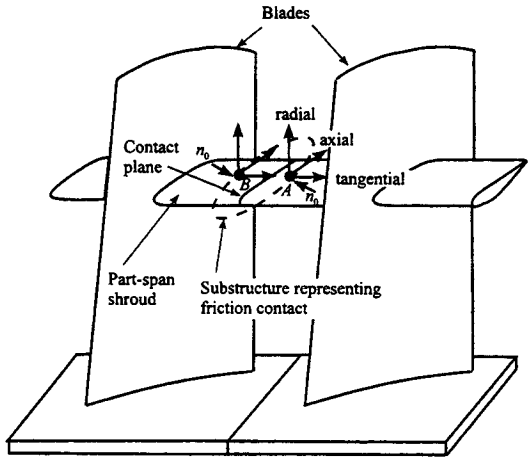

Figure 3 Shroud contact of two neighboring shrouded blades.

$$\mathbf{x} = \begin{bmatrix} x \\ y \\ z \end{bmatrix} = \begin{bmatrix} A_x\sin(\omega t+\phi_x) \\ A_y\sin(\omega t+\phi_y) \\ A_z\sin(\omega t+\phi_z) \end{bmatrix} = \begin{bmatrix} x_s & x_c \\ y_s & y_c \\ z_s & z_c \end{bmatrix} \begin{bmatrix} \sin\omega t \\ \cos\omega t \end{bmatrix} \tag{4}$$

where ω and t are the oscillating frequency and time. For a shrouded blade, several pairs of shroud contact points can be defined. For each pair of shroud contact points, one is on the right and the other left and their motions are denoted as $[\mathbf{x}_r\ \ \mathbf{x}_\ell]^T$.

Since the shrouded blade system is assumed to be tuned, the condition of cyclic symmetry can be applied when deriving the relative motion of a shroud contact. Take the relative motion between the point B of the right shroud and the point A of the left shroud in Figure 3 as an example. First, the motions of the two contact points of the first shrouded blade (left one) are defined and they are $[\mathbf{x}_r\ \ \mathbf{x}_\ell]^T$. Therefore, the motion of point B is now $\mathbf{x}_r$ and the motion of point A differs from $\mathbf{x}_\ell$ with the interblade phase angle (φ). As a result, the relative motion of the two neighboring shrouds, $\mathbf{w}_r$, can be derived.

$$\mathbf{w}_r = \mathbf{T}_1[\mathbf{x}_r\ \ \mathbf{x}_\ell]^T \tag{5}$$

where $\mathbf{T}_1$ is the interblade relative displacement transformation matrix.

$$\mathbf{T}_1 = [\mathbf{I}_{3\times3}\ \ -e^{-j\varphi}\mathbf{I}_{3\times3}] \tag{6}$$

It is worthy noting that only the relative motion at the right shroud contact point is derived. Since the shrouded blade system is assumed to be tuned, the relative motion and the resulting constrained force of the left shroud contact point can be related to those of the right shroud contact point by using the condition of cyclic symmetry. Since both $\mathbf{x}_r$ and $\mathbf{x}_\ell$ are elliptical motions, the resulting relative motion $\mathbf{w}_r$ also has elliptical trajectory in the 3D space.

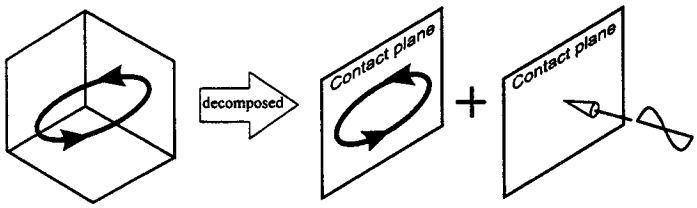

Figure 4 Decomposition of 3D elliptical relative motion.

The elliptical relative motion is often not parallel to the contact plane. In order to analyze the induced friction, the elliptical relative motion in the 3D space can be decomposed into an in-plane elliptical motion on the contact plane and a sinusoidally varying component normal to the contact plane. The in-plane elliptical motion can induce stick-slip friction, and thus can attenuate the resonant response of the shrouded blades. On the other hand, the normal component tends to alter the normal load across the interface; and this effect, in extreme circumstances, may lead to a separation of the interface. This decomposition is shown in Figure 4 schematically. It should be noted that the variable normal load is taken as the sum of the initial contact pressure at equilibrium plus a term that is proportional to the sinusoidally varying normal component of the relative motion. Since this decomposition is to transfer the relative motion from the global coordinate system to the local coordinate system defined in equation (2), it can be carried out by performing a coordinate transformation on the 3D relative motion.

$$\mathbf{u}_r = \mathbf{T}_0^{\mathrm{T}} \mathbf{w}_r \tag{7}$$

Here the 3D relative motion is described in the local coordinate system as follows.

$$\mathbf{u}_r = \begin{bmatrix} v \\ u \\ w \end{bmatrix} = \begin{bmatrix} v_s & v_c \\ u_s & u_c \\ w_s & w_c \end{bmatrix} \begin{bmatrix} \sin\omega t \\ \cos\omega t \end{bmatrix} \tag{8}$$

CONSTRAINED FORCE AT SHROUD CONTACT

After the decomposition, the u and w components of the relative motion follow an elliptical trajectory on the contact plane and can induce the stick-slip friction, while the v component can cause the normal load across the interface to vary dynamically. It is apparent that the u and w motions are coupled together when inducing stick-slip friction. However, the coupling effect of a 2D relative motion having variable normal load on the stick-slip phenomenon is not well understood at this stage. To estimate the equivalent stiffness and damping of a shroud contact experiencing a 2D slip motion and a variable normal load, the first attempt of this study is to use an approximate approach. In this approach, the in-plane elliptical motion is decomposed into two linear motions along the principal major and minor axes of the ellipse. Let u' and w' be the principal major and minor axes respectively. The decoupled relative motion can be derived as follows.

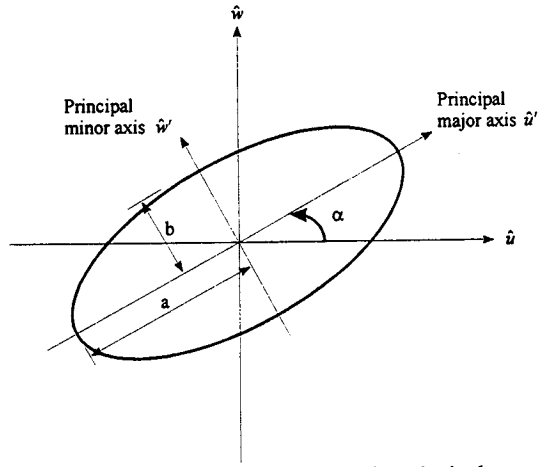

Figure 5 An elliptical trajectory and its principal axes.

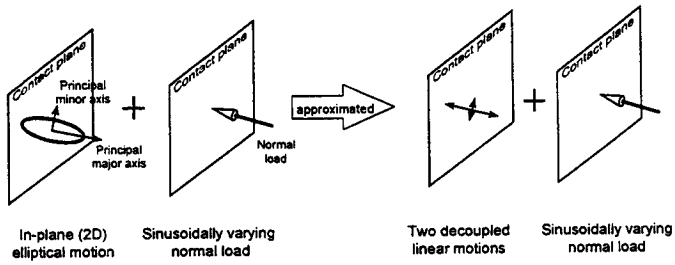

Figure 6 Decoupled in-plane motion.

$$\mathbf{u}_r' = \mathbf{T}_2 \mathbf{u}_r \tag{9}$$

and

$$\mathbf{T}_2 = \begin{bmatrix} 1 & 0 & 0 \\ 0 & \cos\alpha & \sin\alpha \\ 0 & -\sin\alpha & \cos\alpha \end{bmatrix} \tag{10}$$

where $\mathbf{T}_2$ is the decoupling matrix, and α is the inclination of the principle major axis $\hat{u}'$ to the local coordinate axis $\hat{u}$, as shown in Figure 5. Based on the coordinate vector of the relative motion defined in equation (8), the inclination can be established as follows.

$$\alpha = \frac{1}{2}\left\{ \tan^{-1}\left[\frac{u_c + w_s}{u_s + w_c}\right] + \tan^{-1}\left[\frac{w_s - u_c}{u_s + w_c}\right] \right\} \tag{11}$$

The concept of two decoupled linear motions is shown in Figure 6. After the in-plane tangential motion is decoupled into two linear motions, a well developed variable normal load shroud contact model[1] (Yang and Menq, 1996) can be applied separately to each

[1] This shroud contact model has been successfully used in the 2D shroud contact analysis, in which the 2D contact kinematics consists of a linear motion that induces friction and a sinusoidally varying normal component that causes the normal load to alter dynamically.

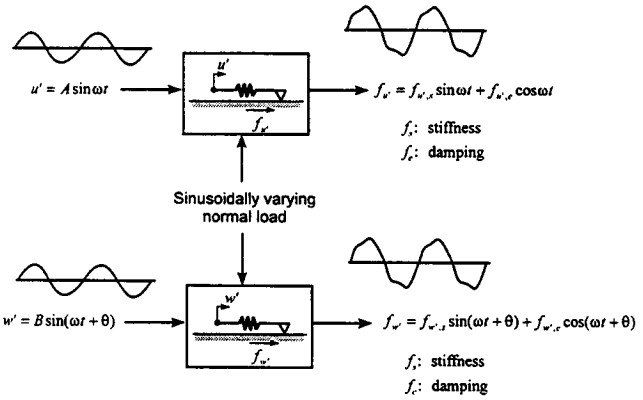

Figure 7 Estimation of effective stiffness and damping.

individual linear motions, and the equivalent stiffness and damping of the shroud contact can be approximately estimated, as shown in Figure 7. Based on this approach, a simplified 3D shroud contact model is developed.

Using the available variable normal load friction force model (Yang and Menq, 1996), the constrained force at the right shroud contact point can be determined. It is a nonlinear function of the decoupled relative motions and can be expressed as follows.

$$\mathbf{p}'_r = \begin{bmatrix} \mathbf{p}'_{rv} \\ \mathbf{p}'_{ru} \\ \mathbf{p}'_{rw} \end{bmatrix} = \begin{bmatrix} \mathbf{p}'_{rv}(v') \\ \mathbf{p}'_{ru}(v',u') \\ \mathbf{p}'_{rw}(v',w') \end{bmatrix} \tag{12}$$

where the nonlinear functions, $\mathbf{p}'_{rv}(v')$, $\mathbf{p}'_{ru}(v',u')$, and $\mathbf{p}'_{rw}(v',w')$, were established in (Yang and Menq, 1996). The constrained force is now defined in the principal directions. It can be transferred to the local coordinate system using the transpose of the decoupling matrix.

$$\mathbf{p}_r = \mathbf{T}_2^{\mathrm{T}}\mathbf{p}'_r \tag{13}$$

Then, the constrained force can be transferred to the global coordinate system as follows.

$$\mathbf{f}_r = \mathbf{T}_0\mathbf{p}_r \tag{14}$$

Furthermore, the constrained forces at a pair of shroud contact points can be related to the force at the right shroud contact point using the interblade relative displacement transformation matrix.

$$\begin{bmatrix} \mathbf{f}_r \\ \mathbf{f}_\ell \end{bmatrix} = \mathbf{T}_1^{\mathrm{H}}\mathbf{f}_r \tag{15}$$

where $\mathbf{T}_1^{\mathrm{H}}$ is the complex conjugate transpose of $\mathbf{T}_1$.

PREDICTION OF RESONANT RESPONSE

The equation of motion of a shrouded blade under a harmonic excitation can be expressed as follows.

$$\mathbf{m}\ddot{\mathbf{x}} + \mathbf{c}\dot{\mathbf{x}} + \mathbf{k}\mathbf{x} = \mathbf{f}_e - \mathbf{f}_N \tag{16}$$

where $\mathbf{x}$ is the nodal displacement vector, $\mathbf{m}$ is the mass matrix, $\mathbf{c}$ is the damping matrix, $\mathbf{k}$ is the stiffness matrix, $\mathbf{f}_e$ is the external harmonic excitation, and $\mathbf{f}_N$ is the nonlinear constrained force which is a nonlinear function of the relative motion at the shroud contact. The finite element model can be three-dimensional and if the model contains n nodes, all the matrices will be $3n \times 3n$ matrices, and all the vectors will be $3n$-element vectors.

The external harmonic excitation can be expressed as follows.

$$\mathbf{f}_e(t) = \mathbf{f}_e e^{j\omega t} \tag{17}$$

where ω is the excitation frequency and $\mathbf{f}_e$ is a complex vector representing the magnitude and phase of the excitation. It is worthy noting that except for the elements associated with those shroud contact points the other elements of $\mathbf{f}_N$ are zeros. It is clear that the nonlinear aspect of the dynamic problem is embedded in the nonlinear friction force $\mathbf{f}_N$. By using the Modal Analysis Method, the mode shape matrix can be obtained and is denoted as Φ. Using the mode shape matrix and the associated modal information, the receptance of the blade can be derived.

$$\mathbf{r} = [r_{k\ell}] = \sum_{i=1}^{3n}\left(\Phi_i \Lambda_i \Phi_i^{\mathrm{T}}\right) \tag{18}$$

and

$$\Lambda_i = \left[\left(\mathbf{k}_i - \omega^2\mathbf{m}_i\right) + j\left(\omega\mathbf{c}_i\right)\right]^{-1} \tag{19}$$

where $r_{k\ell}$ is defined as the steady state response of the k^{th} node due to unit harmonic excitation force at the ℓ^{th} node, Φ_i is the i^{th} mode shape, $\mathbf{m}_i$ is the i^{th} modal mass, $\mathbf{k}_i$ is the i^{th} modal stiffness, and $\mathbf{c}_i$ is the i^{th} modal damping.

When the blade is constrained by its neighboring blades through shroud contacts, the resulting constrained forces are characterized by the displacements of a pair of contact points, $\left[\mathbf{x}_r \quad \mathbf{x}_\ell\right]^{\mathrm{T}}$, and they can be considered as feedback forces that influence the response of the blade. This feedback effect along with the contact kinematics is shown in Figure 8. By using the harmonic balance method, the constrained forces can be approximated by harmonic functions having the same frequency as the external harmonic excitation, and its amplitude and phase are nonlinear functions of the displacements of the pair of contact points. From the nonlinear feedback loop shown in Figure 8, it is evident that in the calculation of nonlinear forced response of a shrouded blade, all the linear degrees of freedom can be condensed to receptance and the modeling of friction contact can be separated from the complex structure model. This approach results in a set of nonlinear algebraic equations, which can be formulated as follows.

$$\begin{bmatrix} \mathbf{x}_r \\ \mathbf{x}_\ell \end{bmatrix} = \mathbf{r}_{ce}\mathbf{f}_e - \mathbf{r}_{cc}\begin{bmatrix} \mathbf{f}_r \\ \mathbf{f}_\ell \end{bmatrix} \tag{20}$$

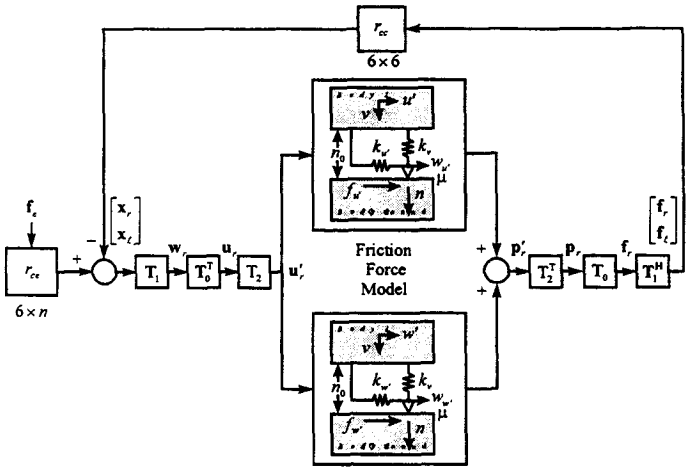

Figure 8 Nonlinear feedback loop and calculation of nonlinear constrained force.

where $[\mathbf{x}_r \quad \mathbf{x}_\ell]^T$ is the nodal displacement vector of the right and left shroud contact points, $[\mathbf{f}_r \quad \mathbf{f}_\ell]^T$ is the resulting constrained force vector, $\mathbf{r}_{ce}$ is the receptance at the shroud contact points due to unit harmonic excitation force, and $\mathbf{r}_{cc}$ is the receptance at the shroud contact points due to unit constrained force.

EFFECT OF 3D SHROUD CONTACT

A shrouded blade system is employed to demonstrate the effect of 3D shroud constraint on the resonant response when compared to 2D shroud constraint. The shrouded blade system is assumed tuned and 20 modes of a single blade are included in the prediction of the resonant response. Each mode shape consists of axial, tangential, and radial components.

The resonant response predicted by using 3D shroud constraint is compared with that predicted by using 2D shroud constraint (Yang and Menq, 1996). Figures 9, 10, and 11 show the prediction of the resonant response when the shroud contact is fully stuck. It is clear that the blade's resonant frequency changes significantly from the region where it is fully slipping, to the region where it is fully stuck. Since 3D shroud constraint provides additional stiffness, the resulting resonant frequency is significantly higher than that predicted using 2D shroud constraint. Figure 9 shows that in the axial direction, in addition to the frequency shift, the amplitude of the resonant response is attenuated to 26.2%, using 3D shroud constraint, and 28.8%, using 2D shroud constraint, when the shroud contact is fully stuck. However, as shown in Figure 10, the amplitude attenuation in the tangential direction is much greater, e.g., attenuated to 0.22%, using 3D constraint, and 0.39%, using 2D constraint. It is evident that the additional stiffness provided by the shroud contact is more significant in the tangential direction than in the axial direction. Figure 11 shows the resonant response in the radial direction. It is clear that when the shroud contact is fully stuck 3D constraint provides additional constraint in the radial direction, therefore, the resonant response is much significantly attenuated.

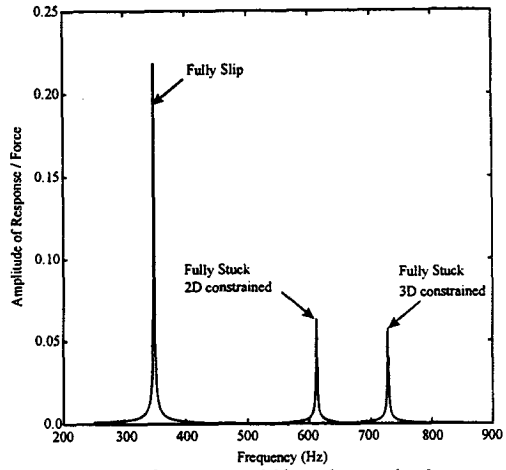

Figure 9 Resonant frequency shift and magnitude attenuation (axial direction).

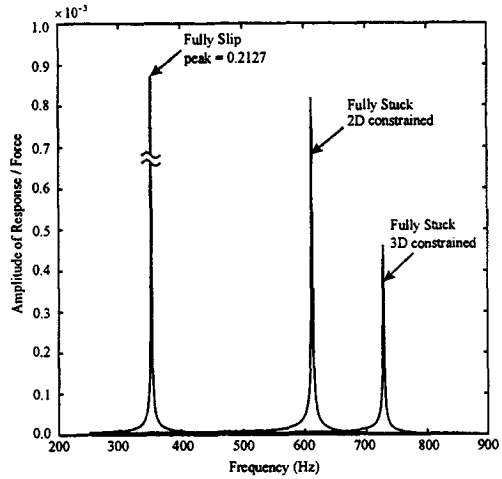

Figure 10 Resonant frequency shift and magnitude attenuation (tangential direction).

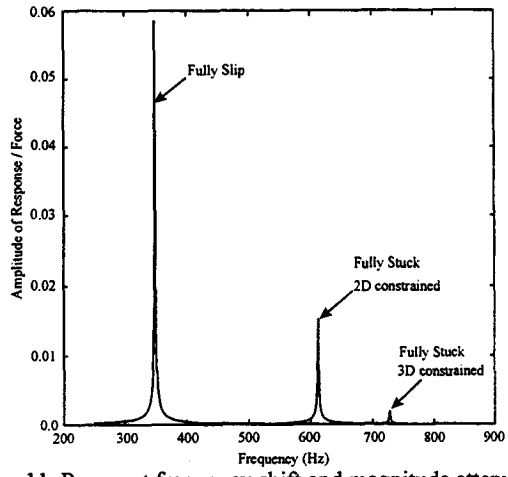

Figure 11 Resonant frequency shift and magnitude attenuation (radial direction).

Figures 12, 13, and 14 show the effect of preload, n_0, on the resonant response in the axial, tangential, and radial directions respectively. It can be seen that when the preload is small the shroud contacts provide mostly damping effect, therefore, the resonant response is attenuated. When increasing preload both damping and stiffness are in effect and the resonant frequency shifts to higher side. However, when the preload becomes too high, damping starts to diminish and the resonant response rises rapidly. In this simulation, $n_0 = 10$ can be considered as the optimal preload, which gives the minimum response.

COMPARISON WITH TIME INTEGRATION METHOD

Since the proposed approach uses two steps of approximation, it is necessary to examine the accuracy of the predicted results. Figures 15 and 16 show the comparison of the predicted results with those of time integration. In these two figures, the predicted results using two dimensional and three dimensional constraint are also compared. Each figure shows three groups of tracking curves. These tracking curves are the predicted resonant response of the shrouded blade system for the cases in which contact preload is relatively high. High contact preload is usually desirable for shroud design. The first group of curves are the predicted results using time integration method and the second group are those of the proposed approach using three dimensional shroud constraint. It can be seen that the proposed approach predicts the frequency and amplitude of the resonant response reasonably well. The third group of curves are the predicted results when applying two dimensional shroud constraint. It is evident that the resonant frequency is underestimated. It can also be seen in Figure 16 that the resonant amplitude in the radial direction is much overestimated when using two dimensional shroud constraint.

CONCLUSION

In this paper, the 3D shroud contact kinematics of a shrouded blade system is studied and a simplified 3D shroud contact model is developed. In this study, the assumed blade motion has three components, namely axial, tangential, and radial components, which result in a three dimensional relative motion at the shroud contact. The resulting relative motion has an in-plane component and the other component perpendicular to the contact plane. The in-plane tangential relative motion can have an elliptical trajectory, and it induces stick-slip friction. On the other hand, the normal relative motion can cause variation of the contact normal load and, in extreme circumstances, separation of the two contacting surfaces.

Using the developed shroud contact model, the equivalent stiffness and damping of the shroud contact can be approximately estimated. With the estimated stiffness and damping, the developed shroud contact model is applied to the prediction of the resonant response of a shrouded blade system. It is shown that since 3D shroud constraint provides additional stiffness, when the shroud contact has high preload and it is near the resign of fully stuck the resulting resonant frequency is significantly higher than that predicted using 2D shroud constraint. It is also shown that when the shroud contact is fully stuck 3D constraint provides additional constraint in the radial direction, therefore, the resonant response in the radial direction is much significantly attenuated.

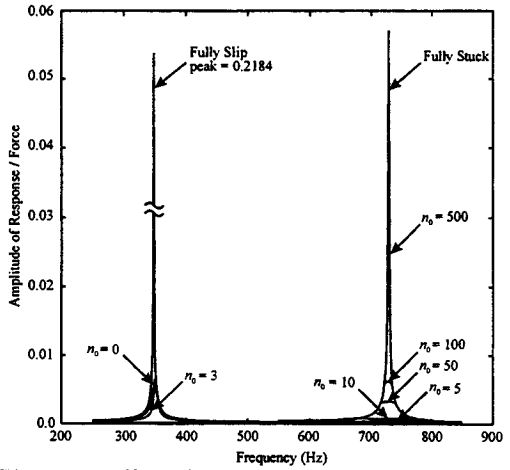

Figure 12 Effect of preload on the resonant response (axial direction)

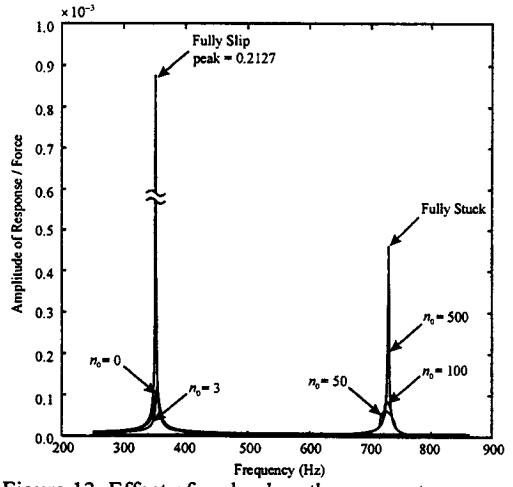

Figure 13 Effect of preload on the resonant response (tangential direction)

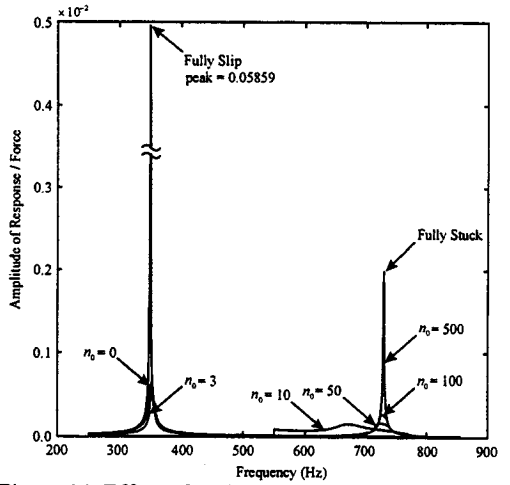

Figure 14 Effect of preload on the resonant response (radial direction)

The effect of preload, n_0, on the resonant response of a shrouded blade system is also studied. It shows that when the preload is small the shroud contacts provide mostly damping effect, therefore, the resonant response is attenuated. When increasing preload both damping and stiffness are in effect and the resonant frequency shifts to higher side. However, when the preload becomes too high, damping starts to diminish and the resonant response rises rapidly.

In order to examine the accuracy of the proposed approach, the predicted results are compared with those obtained using time integration method. It is shown that the proposed approach predicts the frequency and amplitude of the resonant response reasonably well.

ACKNOWLEDGMENT

This material is based on the work supported by the Naval Air Systems Command under Contract NO. N00421-96-C-5145 and by the GUIde Consortium under Contract No. 537934-52253. Any opinions, findings, and conclusions or recommendations expressed in this material are those of the authors and do not necessarily reflect the views of the Naval Air Systems Command or the GUIde Consortium.

REFERENCES

Cameron, T.M., Griffin, J.H., Kielb, R.E., and Hoosac, T.M., 1990, "An Integrated Approach for Friction Damper Design," *ASME Journal of Vibration, Acoustics, Stress, and Reliability in Design*, Vol. 112, Apr., pp. 175-182.

Ferri, A.A., 1996, "Friction Damping and Isolation Systems," *ASME Journal of Vibration and Acoustics*, Vol. 117(B), pp. 196-206.

Griffin, J.H., 1980, "Friction Damping of Resonant Stresses in Gas Turbine Engine Airfoil," *ASME Journal of Engineering for Power*, Vol. 102, Apr., pp. 329-333.

Menq, C.H. and Griffin, J.H., 1985, "A Comparison of Transient and Steady state Finite Element Analysis of the Forced Responses of a Frictionally Damped Beam," *ASME Journal of Vibration, Acoustic, Stress, and Reliability in Design*, Vol. 107, Jan., pp. 19-25.

Menq, C.H., Griffin, J.H., and Bielak, J., 1986, "The Forced Responses of Shrouded Fan Stages," *ASME Journal of Vibration, Acoustic, Stress, and Reliability in Design*, Vol. 108, Jan., pp. 50-55.

Snivasan, A.V. and Cutts, D.G., 1983, "Dry Friction Damping Mechanisms in Engine Blades," *ASME, Journal of Engineering for Power*, Vol. 105, Apr., pp. 332-341.

Williams, E.J. and Earles, S.W., 1974, "Optimization of the Response of Frictionally Damped Beam Type Structures with Reference to Gas Turbine Compressor Blading," *ASME Journal of Engineering for Industry*, Vol. 96, May, pp. 471-476.

Yang, B.D. and Menq, C.H., 1996, "Modeling of Friction Contact and Its Application to the Design of Shroud Contact," ASME Paper No. 96-GT-472, presented at the *International Gas Turbine and Aeroengine Congress & Exhibition*, Birmingham, UK, June 10-13, 1996.

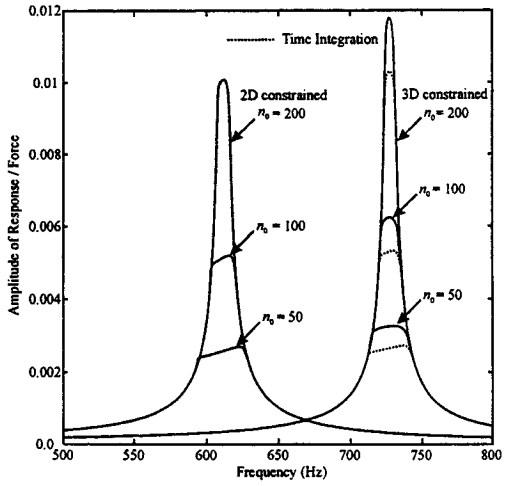

Figure 15 Comparison of resonant responses with time-integration (axial direction).

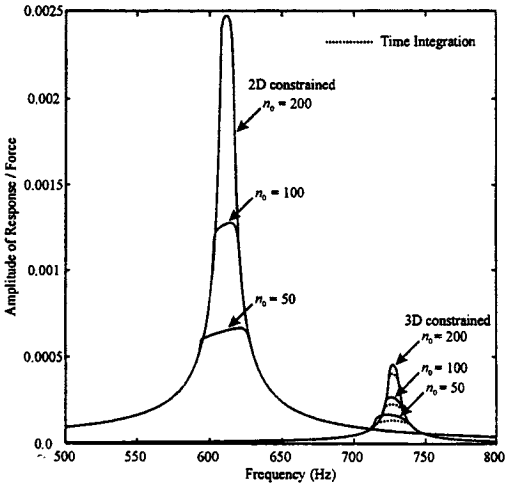

Figure 16 Comparison of resonant responses with time-integration (radial direction).